

## Blind identification of magnetic signals in electron magnetic chiral dichroism using independent component analysis



Jakob Spiegelberg<sup>a,\*</sup>, Dongsheng Song<sup>b,c</sup>, Rafal E. Dunin-Borkowski<sup>c</sup>, Jing Zhu<sup>b</sup>, Ján Rusz<sup>a</sup>

<sup>a</sup> Department of Physics and Astronomy, Uppsala University, Box 516, S-751 20 Uppsala, Sweden

<sup>b</sup> National Center for Electron Microscopy in Beijing, Key Laboratory of Advanced Materials (MOE) and The State Key Laboratory of New Ceramics and Fine Processing, School of Materials Science and Engineering, Tsinghua University, Beijing 100084, China

<sup>c</sup> Ernst Ruska-Centre for Microscopy and Spectroscopy with Electrons and Peter Grünberg Institute, Forschungszentrum Jülich, D-52425 Jülich, Germany

### ARTICLE INFO

#### Keywords:

EMCD  
ICA  
Blind Source Separation  
4D STEM

### ABSTRACT

Electron magnetic chiral dichroism (EMCD) is a promising technique to investigate local magnetic structures in the electron microscope. However, recognition of the EMCD signal, or also finding optimal parameter settings for given materials and sample orientations typically requires extensive simulations to aid the experiment. Here, we discuss how modern data processing techniques, in particular independent component analysis, can be used to identify magnetic signals in an unsupervised manner from energy filtered transmission electron microscopy (EFTEM) images. On the background of the recent advent of 4D scanning transmission electron microscopy, we discuss how this data processing may enable simultaneous tracking of all three spatial components of the magnetic momenta for arbitrary materials and several sample orientations without the previous need of complementary simulations.

Electron energy loss spectroscopy (EELS) offers a wealth of information of the sample down to atomic resolution on modern microscopes. For magnetic samples, the electron magnetic chiral dichroism (EMCD) [1,2] arises from the interaction of the electron with the magnetic moments of the sample in an EELS measurement. The magnetic signal is then obtained either by tuning the phase of the incoming electron, or by detecting electrons scattered into suitable angles. Thus, a successful EMCD measurement offers an opportunity to study nanoscale magnetic devices while at the same time retaining the advantages of EELS measurements, e.g., detailed information of the chemical environment, or site-specific fine-structure differences.

Despite experimental and theoretical advances in recent years pushing the achieved spatial resolution of EMCD measurements from several nanometers to few Ångström [3–13], experimental as well as conceptual challenges remain. Especially for measurements at high spatial resolutions, the low signal to noise ratio (SNR) of the inherently weak EMCD signal renders it difficult to detect (e.g., [4,7,10]). Dependent on multiple parameters, e.g., the sample thickness, convergence and collection angle, phase profile of the electron probe or exact shape and placement of a collection aperture in the objective lens's backfocal plane, the optimization of experimental parameters for a given sample (or material) to achieve the maximal SNR of the EMCD signal remains non-trivial to date.

Today, most studies focus on studying the out-of-plane magnetic moments assuming that the sample is magnetically saturated in the field of the objective lens. Going beyond this restriction to study also the in-plane components of the magnetic field adds an additional layer of complexity since the distribution of the three EMCD components in the backfocal plane overlap strongly. For many samples and crystal orientations, simple placement of a collection aperture at certain places in the backfocal plane may no longer be sufficient to fully distinguish all EMCD contributions.

In this article, we discuss how blind source separation (BSS) methods, in particular independent component analysis (ICA) (e.g., [14] or any other textbook on ICA), can be used to extract contributions to the EMCD signal in *k*-space, as contained in a series of energy filtered diffraction pattern covering the edge of interest, in an unsupervised manner. By applying ICA to both theoretically predicted and experimental data we evaluate the potential and practical applicability of our approach.

In Section 1, we discuss the usage of ICA for recognition of the EMCD signal in more detail. Furthermore, the method is applied to theoretically predicted data. Afterward, in Section 2, we demonstrate the proposed approach experimentally, followed by a brief discussion of the results in Section 3 and an outlook to extend the method to be applied to 4D-STEM data sets in Section 4.

\* Corresponding author.

E-mail address: [jakob.spiegelberg@physics.uu.se](mailto:jakob.spiegelberg@physics.uu.se) (J. Spiegelberg).

<https://doi.org/10.1016/j.ultramic.2018.08.021>

Received 1 March 2018; Received in revised form 23 August 2018; Accepted 25 August 2018

Available online 27 August 2018

0304-3991/ © 2018 Elsevier B.V. All rights reserved.

## 1. Extraction of EMCD using ICA

In order to find a suitable extraction method for the EMCD signal it is useful to consider the mathematical characteristics of its k-space distribution. Experimentally, this distribution can be obtained by acquisition of a series of energy filtered transmission electron microscopy (EFTEM) images of the diffraction plane covering the EELS edge of the magnetic species of interest (see, e.g., [4,15]).

For this purpose, we have computed the k-space distribution of the EMCD signal of a Co crystal in (001) zone-axis (ZA), three beam case orientation (3BC, along the (018) axis) and two beam case orientation (2BC, obtained by successively tilting out of the 3BC so that G-spot and 0-spot have approximately equal intensities, which mimics the experimental setup of 2BCs) using the Mats.V2 code [16]. The crystal was chosen to be 21.72 nm (ZA) and 21.16 nm (3BC, 2BC) thick, the probe had an acceleration voltage of 200 kV. In order to compare EFTEM measurements to STEM experiments we compute both distributions using plane waves as incoming beam as well as convergent probes with a convergence angle of 5 mrad. The resulting distributions of the net non-magnetic and magnetic signals, i.e., the EMCD distributions assuming full polarization along x-, y- or z-axis, are shown in Fig. 1. The z axis was chosen parallel to the beam propagation direction, the sample tilt for the 3BC orientation followed the x axis.

At first sight, the k-space distributions of the EMCD signal are strongly orientation dependent. Additional factors, such as the crystal thickness or the convergence angle, are also known to affect these distributions. However, the z-component appears little correlated to the non-magnetic signal in all crystal orientations studied here. Furthermore, for 3BC and ZA computation, this uncorrelatedness extends to all three EMCD components. Comparing plane wave and convergent beam computations, one notices how the asymmetries of 2BC and 3BC become less pronounced at non-zero convergence angles and are negligible even at the moderate 5 mrad used here.

The origin of this asymmetry has been described before [17,18]. Since 2BC and 3BC imply tilted samples, the Ewald spheres are also correspondingly tilted so that an incoming plane wave will intersect it differently when scattered into the upper or lower half-plane (spanned by the systematic row reflections). When using convergent beams, the beam itself offers a selection of different incoming angles, each with slightly different intersections with the Ewald sphere. Hence, additional changes induced by the sample tilt become less pronounced.

These visual impressions are further corroborated by the correlation coefficients (i.e., Pearson correlation coefficients) shown in Fig. 2, which can easily be estimated from the vectorized component maps of Fig. 1. While the z-component is always uncorrelated to the non-magnetic signal, correlations remain in between the EMCD components for plane waves. At 5 mrad convergence angle, however, the observed correlations are attenuated. For the ZA calculation, all components are orthogonal to each other in either case.

Having recognized the uncorrelatedness of the components, ICA appears to be a suitable blind source separation technique for this unmixing problem. Particularly in cases where the source components, i.e., non-magnetic and EMCD signals, are known to be orthogonal and thus statistically independent, such as the ZA orientation or the 3BC for convergent electron probes, identifiability criteria of ICA are met, the method can be expected to extract the correct, physically meaningful source components. Note that uniqueness of ICA has to be understood as essential uniqueness, i.e., uniqueness up to permutation (ordering of the components) and scaling. Due to the scaling ambiguity, only relative amplitudes of the obtained components can be interpreted directly. To analyze also absolute amplitudes, further normalization with the associated scores is necessary. E.g., when applied to an EFTEM image, the amplitudes of the associated spectra need to be normalized before absolute amplitudes in the extracted k-space distributions can be compared.

A point of criticism of this approach is that while ICA can be

expected to extract the EMCD components, at last, the user needs to identify them as such, which again presupposes knowledge of the EMCD distributions. We suggest to overcome this hurdle by using the following general criteria to identify unknown EMCD contributions

- i. In contrast to non-magnetic signals, EMCD components are not centered around diffraction spots. In particular out-of-plane contributions fulfill this criterion well.
- ii. EMCD contributions tend to be anti-symmetric with regard to some symmetry plane or rotationally symmetric with the rotation axis centered at the 0-spot. Both symmetries are dependent on the crystal orientation and distinguish EMCD contributions from other artifact components.
- iii. Particularly in situations where EMCD contributions and non-magnetic signal are orthogonal, the EMCD contributions vanish when summed over large enough areas. Note that this criterion is likely violated when using electron probes with more general phase profiles, e.g., when using electron vortex beams.

We derive these criteria from our experience with simulations of k-space EMCD distributions across various samples and parameter settings, but point out that they may be violated for some experiment settings. In such cases, further simulations are needed. Yet, as we show below, using these criteria the EMCD contributions may now be identified without prior knowledge.

STEM-EMCD measurements, where the same sample region is scanned several times with different collection aperture placements obtaining spectrum images with EMCD signals of opposing signs, can be considered to yield a 4 dimensional data set,  $\mathcal{X} \in \mathbb{R}^{x \times y \times E \times a}$  where  $x$ ,  $y$ ,  $E$  and  $a$  are the number of pixels along x- and y-axis, the number of energy channels and the number of aperture placements, respectively (the notation  $\mathcal{X} \in \mathbb{R}^{a_1 \times a_2 \times \dots \times a_n}$  denotes a  $n$ -dimensional tensor whose entries are real numbers and whose  $i$ th mode has the length  $a_i$ ). One may thus wonder whether ICA, when applied to the matrixized data  $\mathbf{X} \in \mathbb{R}^{(x \cdot y \cdot E) \times a}$ , can be used to extract the EMCD signal also here. Unfortunately, the typically low number of aperture placements  $a$  may be lower than the number of source spectra. The thus arising rank deficiency would prohibit ICA to fully separate magnetic and non-magnetic contributions. Furthermore, the averaging of large k-space regions, which is implicitly done by usage of a collection aperture, may destroy the statistical independence of the components (depending on the sample orientation and exact placement of the collection apertures). Hence, ICA applied to the k-space components may not offer a general route to EMCD extraction in STEM-EMCD measurements.

## 2. EMCD extraction on experimental data

In this section, we will demonstrate how ICA in combination with the above three criteria is able to identify the EMCD contributions in EFTEM images measured on a Co crystal tilted in two- (2BC) and three-beam case orientation and an Yttrium-iron garnet (YIG) tilted to ZA orientation. All three being typical crystal orientations used in EMCD measurements.

The samples used in the experiments are a Co nanoplate [13] and a YIG single crystal [19]. The energy filtered diffraction patterns for Co and YIG were acquired using a Gatan GIF spectrometer on a FEI Titan 80–300 operated at 300 kV with the energy step of 1 eV (slit width 2 eV). The acquisition time for each frame with a size of  $1024 \times 1024$  is set to 10 s to ensure the signal-noise-ratio. The energy ranges in the experiments for Co and YIG are chosen around the L-edges of Fe and Co, respectively, i.e., 660–780 eV and 720–870 eV. The diameter of the (parallel) electron beam is about 100 nm. The thickness of the probed regions are approx. 20 nm for Co and approx. 45 nm for YIG. The three-dimensional data sets are consisting of the reciprocal  $k_x$ - $k_y$  plane and electron energy loss. The artifacts and distortions are corrected for all the data sets. Firstly, the X-ray spikes are removed for all frames. Then,

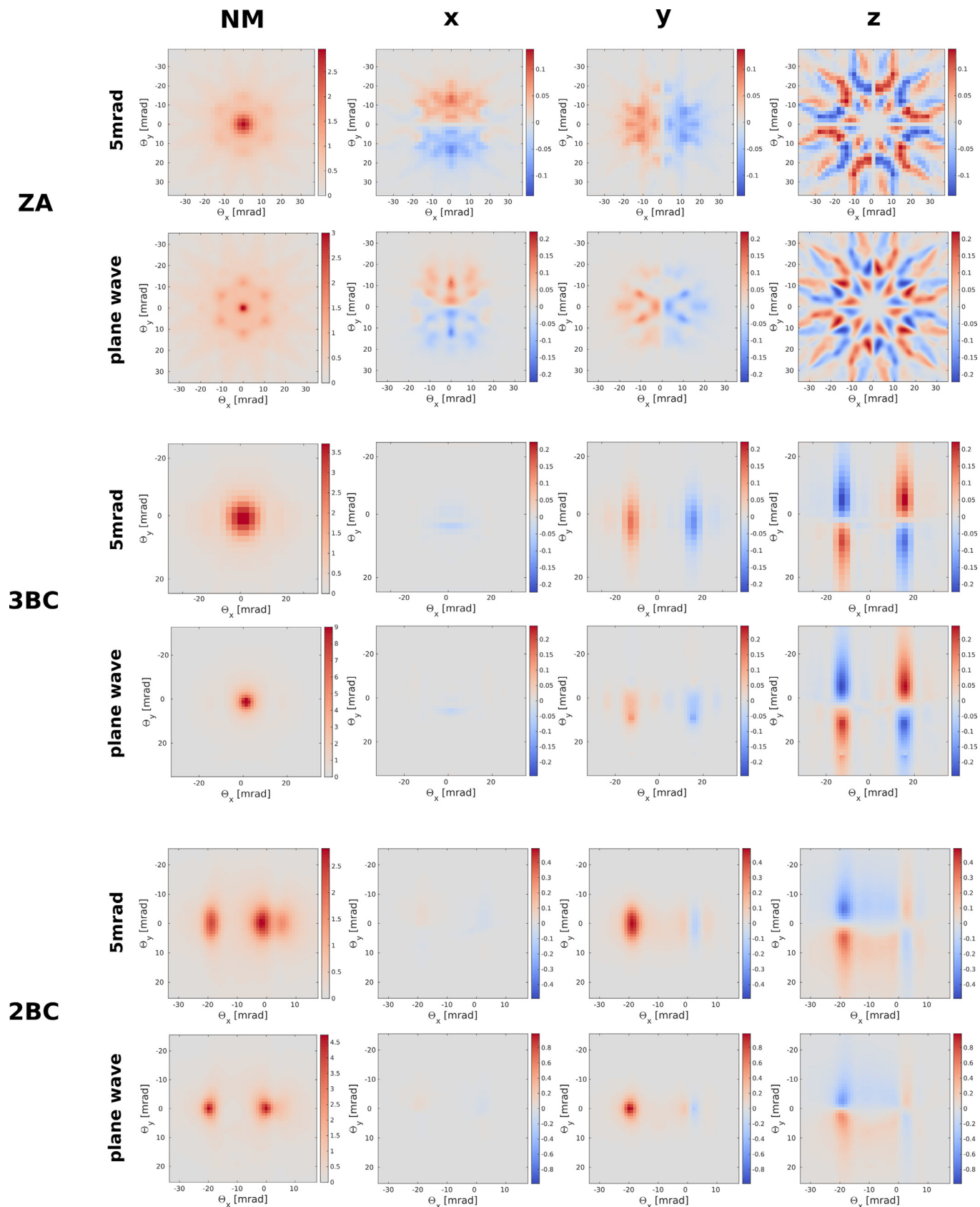


Fig. 1. Theoretically predicted k-space distributions of the EMCD signal and net non-magnetic signal for a Co crystal in zone axis orientation (top), 3 beam orientation (center) and 2 beam orientation (bottom), each using a plane wave and 5 mrad convergence angle. All intensities are in arbitrary units.

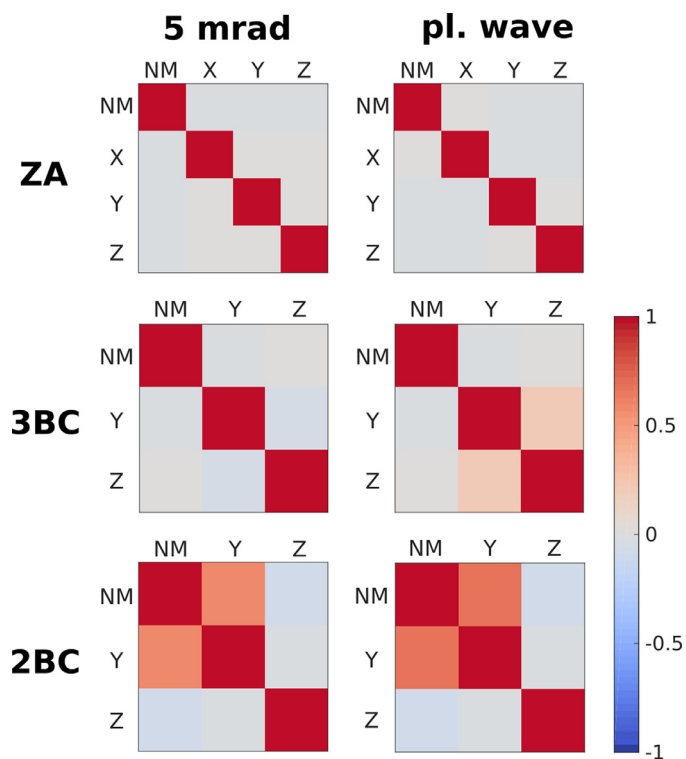


Fig. 2. Correlation coefficients for the non-magnetic (NM) and 3 EMCD (X,Y,Z) components for the three sample orientations and convergence angles displayed in Fig. 1. The x-components of the 3BC and 2BC simulation were omitted due to the negligibly small amplitudes making them experimentally intractable. Note also that pronounced negative correlation coefficients may occur for other settings, e.g., flipped magnetization directions.

the SDSD (Statistically Determined Spatial Drift) script [20] installed in Digital Micrograph is used to conduct the automated spatial drift correction for EFTEM image series by selecting the transmitted spot as a reference. At last, non-isochromaticity of the data sets are corrected according to the peak of the  $L_3$  edges of Co and Fe [21].

### 2.1. Co, two beam case

The first example studied here is the Co crystal oriented to 2BC orientation. The EFTEM set was aligned and then background subtracted by fitting a power law model in the pre-edge using the background subtraction scheme from [22] (fitted in the range from 741–760 eV). Afterwards, each energy slice was filtered using a broad Gaussian filter (with  $\sigma = 20$ ). Principal component analysis (PCA) indicates 6 significant components on the thus pre-processed data set. ICA was applied to the scores obtained via PCA, the resulting components are shown in Fig. 3.

Now applying the three selection criteria outlined in Section 1, one can exclude components a, b, c since they are centered around the remaining diffraction spots. Components d and e can similarly be excluded since they lack major negative contributions in the distribution map, thus violating the third criterion. The remaining component (f) indeed resembles the typical EMCD distribution for a fully z-polarized sample.

Also considering the associated spectrum, shown in Fig. 4, one does not obtain the EMCD spectrum immediately, which may hint to remaining mixing and the influence of artifact components, but can nonetheless visualize the EMCD spectrum by comparison to the mean spectrum. The classical branching of  $L_3$  and  $L_2$  edge intensity is observed.

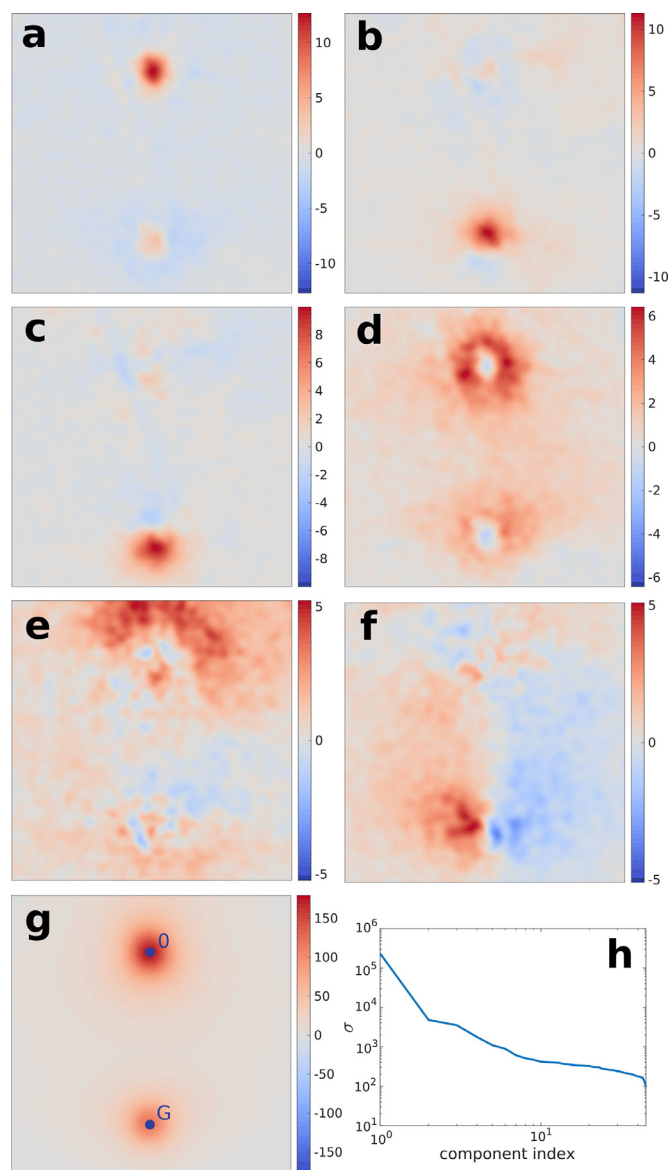


Fig. 3. Source components unmixed using ICA on an EFTEM series measured on a Co crystal in 2 beam orientation as well as the mean intensity of the background subtracted data set (g) and the scree plot obtained by PCA (h). The intensities are in arbitrary units.

### 2.2. Co, three beam case

Next, we consider an EFTEM set of a Co crystal in 3BC orientation. The data were pre-processed analogously to the previous section, i.e., aligned, background subtracted and then filtered by a Gaussian filter ( $\sigma = 20$ ) in every energy slice. PCA suggested a total of 11 significant components, the components obtained by subsequent ICA are displayed in Fig. 5.

As before, we apply the three selection criteria to the obtained components. Components e, f, g, h and i are localized around the three diffraction spots and can thus be excluded. Components j and k lack any obvious symmetry and can thus similarly be excluded. Among the remaining components, b, c and d correlate strongly with the four quadrants of which the CCD camera is composed. Additionally assuming that the EMCD map is independent from these artifacts allows to neglect also these components. The only remaining component (a) again resembles the expected EMCD distribution closely (comp. Fig. 1).

As before for the 2BC, the EMCD spectrum is not obtained directly.

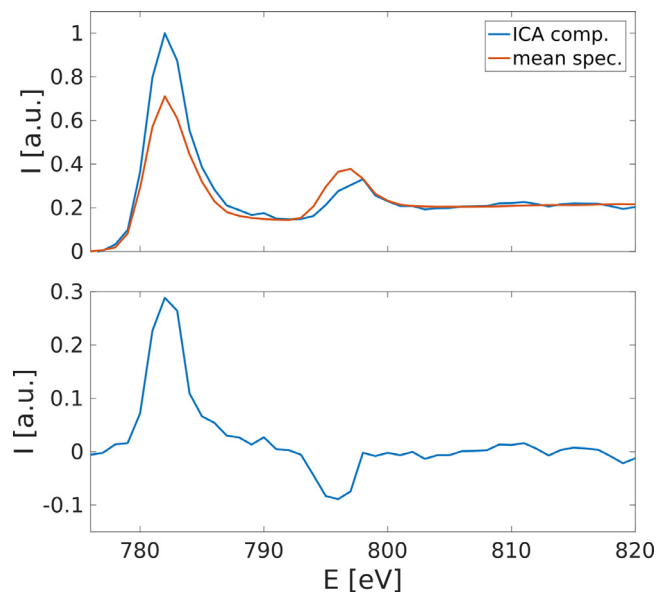


Fig. 4. Normalized spectral signatures of the independent component carrying the EMCD signal and the mean spectrum (top) as well as their difference (bottom). The spectrum corresponds to component f in Fig. 3.

Instead, as shown in Fig. 6, a comparison of the associated spectrum with the mean spectrum can be used to display the characteristic branching of  $L_3$  and  $L_2$  peaks.

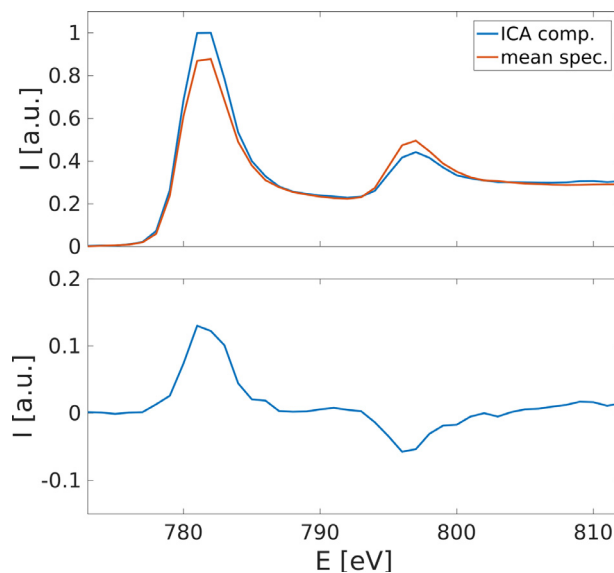


Fig. 6. Normalized spectral signatures of the independent component carrying the EMCD signal and the mean spectrum (top) as well as their difference (bottom). The spectrum corresponds to component a in Fig. 5.

### 2.3. YIG, zone axis orientation

The last sample considered here is the ZA data set acquired on YIG. EMCD signals have previously been extracted from this sample, a comparison to theoretically predicted EMCD maps can be found in [19].

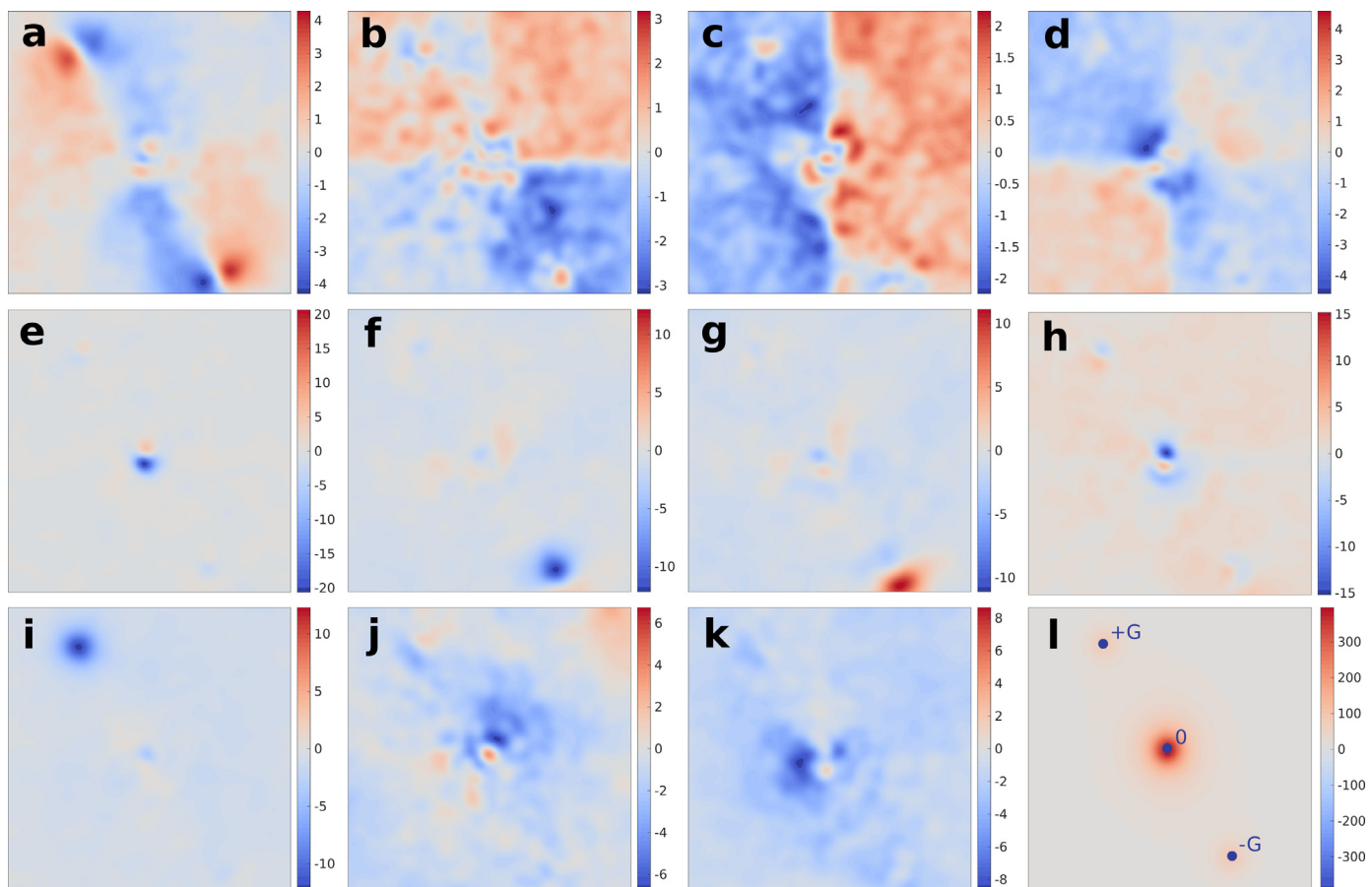
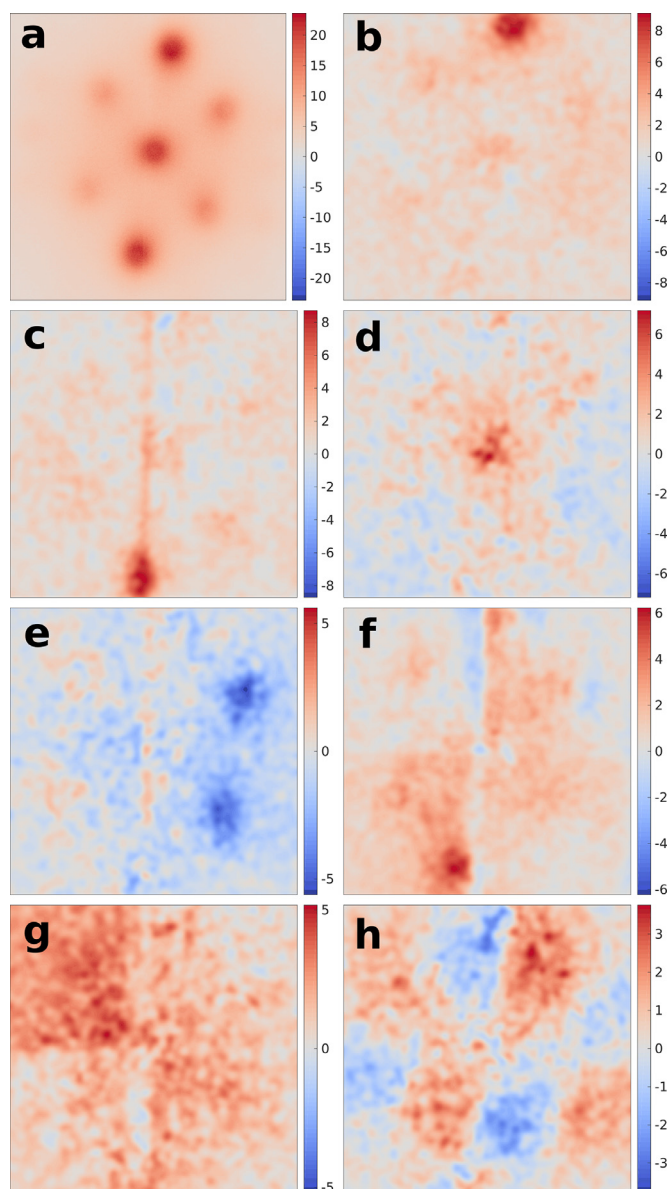


Fig. 5. Source components unmixed using ICA on an EFTEM series measured on a Co crystal in 3BC orientation as well as the mean intensity of the background subtracted data set (l). The intensities are in arbitrary units.



**Fig. 7.** Mean intensity of the background subtracted EFTEM set (a) and source components unmixed using ICA (b to h) on an EFTEM series measured on a YIG crystal in ZA orientation. The intensities are in arbitrary units.

In analogy to the previous two data sets, the data were aligned, background subtracted and Gaussian filtered ( $\sigma = 10$ ,  $\sigma$  is chosen smaller than for the 2BC and 3BC since the EMCD distribution is expected to fluctuate with a higher spatial frequency) before being subjected to PCA, which indicated 7 significant components. The resulting independent components are displayed in Fig. 7.

Excluding components centered around diffraction spots (d and e), components without obvious symmetry (b, c and f) and components consisting of positive (negative) values only (g) leaves only one component as EMCD candidate. Note how also this data set shows components which seem unrelated to the diffraction signals and seem to be some spurious contribution of the detection system, i.e., the stripe-like feature of components c and f.

The spectrum of component h is shown in Fig. 8. In this case the EMCD spectrum appears immediately without additional comparison with the mean spectrum, having a comparable spectral shape (and distribution) as shown in [19].

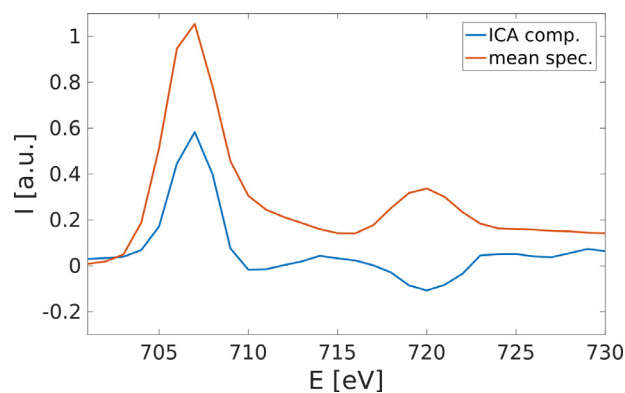


**Fig. 8.** Normalized spectral signatures of the independent component carrying the EMCD signal and the mean spectrum. The spectrum corresponds to component h in Fig. 7.

### 3. Discussion

The three data sets treated in the previous section can serve as a proof of principle of the capability of ICA to identify EMCD components in energy filtered diffraction image series in a widely autonomous manner. In all three cases the qualitatively correct EMCD distribution was extracted. However, the expectation to directly extract the EMCD distribution and spectrum was not met. Instead, additional contrasting of the obtained components to the mean spectrum was necessary to visualize the EMCD spectrum for the Co sample. We also observe that all three data sets display artifact components. In the first set (Fig. 3), components b and c likely originate from slight misalignments of the G-spot by minor changes of the crystal tilt in between acquisition of individual energy slices. For the latter two sets, similar components are observed besides additional camera artifacts, as discussed above. A quantitative analysis of these three data sets may thus be prohibited due to residual mixing of EMCD and artifact components. The unmixing performance of ICA hinges on the independence of the signal of interest from all other signals - non-magnetic and artifact signals alike. Since one can not warrant that artifact components will be independent of the magnetic signal, ICA can not offer a guarantee for successful unmixing of EMCD from them.

Turning this observation around, we see that while this extraction approach is *sensitive* to misalignment, changes of sample tilt and camera artifacts in the sense that more components arise, it is also *robust* to such error sources, as the qualitative EMCD maps could be extracted in spite of the data's shortcomings. For future measurements on more stable microscopes equipped with less artifact prone cameras these error sources will likely be negligible, the fully quantitative unmixing theoretically possible (based on the observations of Section 1) may be achieved.

Already now the achieved qualitative unmixing poses a way to, e.g., experimentally optimize the collection aperture placement for a subsequent STEM-EMCD measurement. Even in cases where several EMCD contributions overlap, e.g., in case different lattice sites contribute with different EMCD signals, ICA may allow to track all signals simultaneously.

### 4. ICA for 4D-STEM EMCD

If not for the sample's magnetic polarization due to the field of the objective lens, the three EMCD components may vary freely in an experiment, they can be expected to appear mixed. While, e.g., the 3BC orientation allows for extraction of y and z component via suitable placement of a circular collection aperture, this is less straightforward for the ZA orientation. Besides presupposing knowledge of optimal aperture placements, this procedure would require several

measurements of the same sample region with different apertures in order to get a complete picture of the sample's magnetism, which is time consuming and wasteful with the electron counts. If, however, one would instead acquire a 4D-STEM data set containing EFTEM images at every pixel of the STEM image [23,24], all moment directions can be tracked simultaneously due to the unmixing through ICA.

In such a 4D-STEM measurement, an energy slit needs to be placed to select, e.g., the  $L_3$  edge only, different pixels of the 4D-STEM set with different magnetization directions will then have correspondingly different weights of the three different EMCD contributions. ICA on the compressed data set may then extract them. I.e., above we have treated data sets  $\mathcal{X} \in \mathbb{R}^{k_x \times k_y \times E}$ , where  $k_x$  and  $k_y$  denote the k-space grid of the EFTEM image and  $E$  the number of energy channels. The sets were matricized to  $\mathbf{X} \in \mathbb{R}^{k_x \cdot k_y \times E}$  so that a matrix factorization technique (here ICA) yields basis vectors of the vectorized k-space maps assuming that the EMCD component weights vary over the spectral range considered. For a 4D-STEM set,  $\mathcal{X} \in \mathbb{R}^{x \times y \times k_y \times k_x}$  ( $x$  and  $y$  being the real space grid), a matricization to  $\mathbf{X} \in \mathbb{R}^{x \cdot y \times k_y \cdot k_x}$  with subsequent matrix factorization similarly yields the vectorized k-space maps now assuming that the weights of the EMCD components vary across different pixels in the data set rather than in different energy channels. Rather than measuring EMCD spectra, such a measurement would yield position dependent amplitudes of the magnetic moment direction components. Domain walls, spin spirals and other non-trivial spin arrangement could be studied efficiently.

Among the practical issues of this approach is an energy filter selecting the magnetic species of interest, e.g., the Co  $L_3$ -edge in the examples studied above. Furthermore, we expect the approach to be sensitive to sample thickness and orientation changes, much as the EFTEM image is sensitive to these two parameters. I.e., different thicknesses or orientations would likely need to be described by a different set of components, thus complicating the analysis.

While microscopes capable of 4D-STEM measurements are scarce as of today, the proposed measurement is an experimentally otherwise straightforward approach to get a complete picture of the samples magnetism using EMCD. ICA aided extraction of EMCD signals opens thus exciting new possibilities to study nanoscale magnetism.

## 5. Conclusions

In this article we have demonstrated how ICA can be used to extract EMCD contributions from a series of energy filtered diffraction patterns. By means of three simple selection criteria, the EMCD contribution can be identified without prior knowledge for several typical measurement setups. This opens the possibility to employ EMCD measurements in a more automatized manner not requiring additional simulations for parameter optimization or guidance of the EMCD extraction.

When applied to experimental data sets, we obtain a qualitatively correct unmixing, robust to artifacts arising from shortcomings of the experimental equipment. A fully quantitative analysis of the data was prohibited due to the presence of these additional components, which is a hurdle likely overcome in future measurements.

An outlook considering recent experimental developments was given. The here outlined method may prove useful to enable facile measurements of the magnetic momenta along all spatial modes or

identification of several contributing magnetic species in parallel, neither of which can currently be performed in the electron microscope with ease.

## Acknowledgments

J.S. and J.R. acknowledge financial support from the Center of Interdisciplinary Mathematics (CIM) at Uppsala University, the Swedish Research Council and the Göran Gustafssons Foundation. D.S. thanks Wenting Huang and Gunther Richter from the Max Planck Institute for Intelligent Systems for providing the Co nanoplate and Jianwang Cai from the Institute of Physics, Chinese Academy of Sciences for providing the YIG sample. D.S. also thanks Bernhard Schaffer for providing the SDDS script. This work was financially supported by the Chinese National Natural Science Foundation (11374174, 51390471, 51527803) and National 973 Project of China (2015CB654902). The work made use of the resources of the Ernst Ruska-Centre for Microscopy and Spectroscopy with Electrons in Jülich and the National Center for Electron Microscopy in Beijing. The research leading to these results received funding from the European Research Council under the European Union's Seventh Framework Programme (FP7/2007-2013)/ERC grant agreement number 320832.

## References

- [1] C. Hébert, P. Schattschneider, *Ultramicroscopy* 96 (2003) 463–468.
- [2] P. Schattschneider, S. Rubino, C. Hébert, J. Ruzs, J. Kuneš, P. Novák, E. Carlino, M. Fabrizio, G. Panaccione, G. Rossi, *Nature* 441 (2006) 486.
- [3] P. Schattschneider, M. Stöger-Pollach, S. Rubino, M. Sperl, C. Hurm, J. Zweck, J. Ruzs, *Phys. Rev. B* 78 (2008) 104413.
- [4] H. Lidbaum, J. Ruzs, A. Liebig, B. Hjörvarsson, P. Oppeneer, E. Coronel, O. Erikson, K. Leifer, *Phys. Rev. Lett.* 102 (2009) 037201.
- [5] J. Verbeeck, H. Tian, P. Schattschneider, *Nature* 467 (2010) 09366.
- [6] P. Schattschneider, B. Schaffer, I. Ennen, J. Verbeeck, *Phys. Rev. B* 85 (2012) 134422.
- [7] S. Muto, J. Ruzs, K. Tatsumi, R. Adam, S. Arai, V. Kocevski, P. Oppeneer, D. Bürgler, C. Schneider, *Nat. Comm.* 5 (2014) 3138.
- [8] J.C. Idrobo, J. Ruzs, J. Spiegelberg, M.A. McGuire, C.T. Symons, R.R. Vatsavai, C. Cantoni, A.R. Lupini, *Adv. Chem. Struct. Imaging* 2 (2016) 5.
- [9] J. Ruzs, S. Muto, J. Spiegelberg, R. Adam, K. Tatsumi, D.E. Bürgler, P.M. Oppeneer, C.M. Schneider, *Nat. Comm.* 7 (2016) 12672.
- [10] T. Thersleff, J. Ruzs, B. Hjörvarsson, K. Leifer, *Phys. Rev. B* 94 (2016) 134430.
- [11] D. Song, G. Li, J. Cai, J. Zhu, *Sc. Rep.* 6 (2016) 18489.
- [12] A. Edström, A. Lubk, J. Ruzs, *Phys. Rev. B* 94 (2016) 174414.
- [13] D. Song, A.H. Tavabi, Z.A. Li, A. Kovács, J. Ruzs, W. Huang, G. Richter, R.E. Dunin-Borkowski, J. Zhu, *Nat. Commun.* 8 (2017) 15348.
- [14] P. Comon, C. Jutten, *Handbook of Blind Source Separation, Independent Component Analysis and Applications*, Academic Press, Oxford, 2010.
- [15] B. Warot-Fonrose, F. Houdellier, M.J. Hÿtch, L. Calmels, V. Serin, E. Snoeck, *Ultramicroscopy* 108 (2008) 393–398.
- [16] J. Ruzs, *Ultramicroscopy* 177 (2017) 20.
- [17] J. Ruzs, P. Oppeneer, H. Lidbaum, S. Rubino, K. Leifer, *Microscopy* 237 (2010) 465–468.
- [18] D. Song, Z. Wang, J. Zhu, *Ultramicroscopy* 148 (2015) 42–51.
- [19] D. Song, J. Ruzs, J. Cai, J. Zhu, *Ultramicroscopy* 169 (2016) 44.
- [20] B. Schaffer, W. Grogger, G. Kothleitner, *Ultramicroscopy* 102 (2004) 27–36.
- [21] C. Gatel, B. Warot-Fonrose, P. Schattschneider, *Ultramicroscopy* 109 (2009) 1465–1471.
- [22] J. Spiegelberg, J. Ruzs, K. Leifer, T. Thersleff, *Ultramicroscopy* 181 (2017) 117–122.
- [23] C. Ophus, P. Ercius, M. Sarahan, C. Czarnik, J. Ciston, *Microsc. Microanal.* 20 (2014). Suppl. 3
- [24] H. Yang, L. Jones, H. Ryll, M. Simson, H. Soltau, Y. Kondo, R. Sagawa, H. Banba, I. Maclaren, P. Nellist, *J. Phys.: Conf. Ser.* 644 (2015) 012032.